Solid State Sciences 109 (2020) 106394

Contents lists available at ScienceDirect

Solid State Sciences

journal homepage: http://www.elsevier.com/locate/ssscie

Salt-flux synthesis, crystal structure and theoretical characterization of $Rb_{0.74}Ga_{6.62}Ti_{0.38}O_{11}$

Mohammad Usman [a], Vancho Kocevski [b], Mark D. Smith [a], Theodore Besmann [b], Hans-Conrad zur Loye [a,*]

[a] Department of Chemistry and Biochemistry, University of South Carolina, Columbia, SC, 29208, United States
[b] Department of Mechanical Engineering, University of South Carolina, Columbia, SC, 29208, United States

ARTICLE INFO

Keywords:
Rubidium gallium titanate
Molten salt flux synthesis
Crystal structure
DFT calculations

ABSTRACT

Single crystals of $Rb_{0.74}Ga_{6.62}Ti_{0.38}O_{11}$ (RGTO) were grown from a mixed RbCl–RbF flux at 850 °C. The compound crystallizes in the $RbGa_7O_{11}$ structure type, which is reminiscent of the hollandite and β-Ga_2O_3 structure types. RGTO crystallizes in the monoclinic space group $P2/m$ with lattice parameters a = 8.3355 (8) Å, b = 3.0286 (3) Å, c = 9.5028 (9) Å, and β = 114.620 (3)°. The crystal structure of RGTO is comprised of GaO_6 and mixed $(Ga/Ti)O_6$ octahedra and GaO_4 tetrahedra connected in a complex three-dimensional, anionic framework exhibiting eight-sided channels that are occupied by disordered Rb cations required for charge balance. First-principles calculations in the form of density functional theory were performed, which indicated the complex to be a charge transfer semiconductor.

1. Introduction

A large variety of materials crystallize in porous, three-dimensional structure types, including main group element containing structures, such as zeolites, and transition metal containing structures, such as the hollandite tunnel structure. Hollandites, described by the general formula $A_xM_8O_{16}$ (A = alkali or alkaline earth ions and M = di, tri or tetravalent cations), represent one class of porous framework materials containing channels filled by mono- or divalent cations. The combination of the tunnel structure and the variable composition has led to the application of hollandites in a number of different areas [1–5].

A particularly important area for hollandite oxides is their use as efficient waste forms in nuclear waste disposal [6–9]. Crystalline ceramic wasteforms, such as SYNROC and titanate/alumina based ceramics can incorporate a broad spectrum of chemical species within their structures, resulting in relatively high waste loadings. Furthermore, they are resistant to hydrothermal leaching [10–12]. The hollandite phase, $A_xM_8O_{16}$, contains channels due to the arrangement of edge sharing chains of dimers that can hold +1 and + 2 cations depending on the charge of the metal cations occupying the octahedral sites. The titanium based hollandite, A_x $(Ti^{4+}, M)_8O_{16}$, is of interest as a waste form due to favorable leach resistance and its ability to immobilize cesium in the structure [13]. This interest has led a number of groups, including ours, to explore structures related to the hollandite structure by changing the cations occupying the octahedral sites.

Among the hollandites, there are only a limited number of gallium-based compositions known that contain K or Ba as the A-site cation, making it of interest to determine if other gallium-based systems that incorporate larger alkali cations and that crystallize in the hollandite or related structure types can be synthesized [14,15]. Utilizing exploratory flux crystal growth, $Rb_{0.74}Ga_{6.62}Ti_{0.38}O_{11}$ (RGTO) was isolated in a reaction intended to crystallize a Rb-Ga-Ti-O hollandite [16]. Upon solving the structure, it was found that RGTO does not crystallize in the hollandite structure type, but interestingly, displays higher structural complexity in the form of a three-dimensional framework featuring large eight-sided channels, in contrast to the (2 × 2) channels characteristic of the hollandite framework. This structure type was first observed in our recently reported $CsGa_7O_{11}$ and $RbGa_7O_{11}$, which crystallize in this new hollandite reminiscent, structure type [17]. RGTO is best thought of as a transition metal doped version of the parent $RbGa_7O_{11}$ phase.

Herein, we report on the molten flux synthesis, structure determination, and ion exchange experiments of RGTO. First-principles calculations in the form of density functional theory were performed to establish the stability of RGTO and of ion exchanged compositions.

* Corresponding author.
E-mail address: zurloye@mailbox.sc.edu (H.-C. zur Loye).

https://doi.org/10.1016/j.solidstatesciences.2020.106394
Received 23 July 2020; Received in revised form 21 August 2020; Accepted 23 August 2020
Available online 27 August 2020
1293-2558/© 2020 Elsevier Masson SAS. All rights reserved.

2. Experimental section

2.1. Materials and methods

GaF_3 (99.5%, BTC), TiO_2-rutile (99.9%, Alfa Aesar), RbCl (99%, Alfa Aesar) and RbF (99.1%, Alfa Aesar) were used as received for the synthesis of RGTO. RGTO was prepared by layering a mixture of 0.065 g of GaF_3 and 0.04 g of TiO_2 beneath 1 g of a eutectic mixture of RbCl–RbF in a 7.5 cm tall by 1.2 cm diameter cylindrical silver crucible with one of its ends sealed and welded shut. The other end of the crucible containing the charge was crimped shut and the loaded crucible was placed into a programmable furnace. The reaction mixture was heated at 10 °C/min to 850 °C, maintained at this temperature for 12 h, slow cooled at 0.17 °C/min to 500 °C, and then rapidly cooled to room temperature by shutting the furnace off. Once cooled to ambient temperature, the solidified RbCl–RbF flux was dissolved in hot distilled water, aided by sonication, and the resulting products were isolated via vacuum filtration. Colorless rods of RGTO (approximate dimensions 0.100 × 0.060 × 0.040 mm^3) were obtained in about 20% yield.

Ion exchange experiments were carried out by layering 0.1 g of RGTO crystals under 1 g of ANO_3 (A = K and Cs) salt and holding the mixture at 350 °C for 16 h before removing without cooling. The crystals were isolated by vacuum filtration.

2.2. Single crystal X-ray diffraction

X-ray intensity data from a colorless rod were collected at 301 (2) K using a Bruker D8 QUEST diffractometer equipped with a PHOTON 100 CMOS area detector and an Incoatec microfocus source (Mo Kα radiation, $\lambda = 0.71073$ Å) [18]. The data collection covered 99.8% of reciprocal space to $2\theta_{max} = 75.6°$, with an average reflection redundancy of 8.4 and $R_{int} = 0.030$ after absorption correction. The raw area detector data frames were reduced, scaled and corrected for absorption effects using the SAINT+ and SADABS programs [18,19]. Final unit cell parameters were determined by least-squares refinement of 7683 reflections taken from the data set. An initial structural model was obtained with SHELXT [20]. Subsequent difference Fourier calculations and full-matrix least-squares refinement against F^2 were performed with SHELXL-2018 using the ShelXle interface [21].

The compound crystallizes in the monoclinic system. The pattern of systematic absences in the intensity data ruled out the presence of a screw axis or glide plane. The space group $P2/m$ was found by SHELXT and was confirmed by structure solution. The asymmetric unit consists of three disordered rubidium atom sites, two pure gallium sites, two mixed gallium/titanium sites and six unique oxygen atom sites. Most atoms are located on mirror planes: atoms Rb (2), Ga (1), O (1), O (5) and O (6) occupy site 2 *m* and atoms Rb (3), Ga (2), Ga (3)/Ti (3) and O (2)–O (4) occupy site 2*n*. Ga (4)/Ti (4) is located on site 1*g* with 2/*m* site symmetry, and Rb (1) is located on a general position (site 4*o*). The rubidium atoms are disordered along columns parallel to ***b***. Three unique, partially occupied Rb sites were identified, Rb (1)–Rb (3). Rb (1) is the dominant site, with a refined site occupancy factor (*sof*) of 0.160 (5). The Rb (2) and Rb (3) occupancies refined to 0.04 (1) and 0.007 (2), respectively. These are near zero, but omitting them resulted in unacceptably large Rb (1) displacement parameters and significant difference map peaks in the region. No significant deviation from unity occupancy was observed for the Ga (1) and Ga (2) sites. The Ga (3) and Ga (4) sites refined to less than full occupancy, *sof* (Ga3) = 0.962 (3) and *sof* (Ga4) = 0.929 (3). This was interpreted as mixing of the lighter atom titanium onto these two sites. A model with both sites constrained to full occupancy by a Ga/Ti mixture was refined, yielding *sof* (Ga3/Ti3) = 0.901 (7)/0.099(7) and *sof* (Ga4/Ti4) = 0.817(9)/0.183(9). Oxygen atom O (6) was initially located on the origin (site 1*a*), but this caused a highly prolate displacement parameter (U3/U1 = 6.0). A split position, located on the mirror plane of site 2*d* but disordered across the origin and half-occupied, gave a stable refinement with a more acceptably spherical displacement parameter (U3/U1 = 3.9). As formulated, the refinement model does not charge balance but generates a small positive charge of +0.12 e^-, indicating a deficiency in the refinement model. The reason for the deviation from electroneutrality is unknown, but may arise from an inaccurate Ga/Ti mixing or rubidium disorder model, possibly involving unidentifiable vacancies. All atoms were refined with anisotropic displacement parameters except for the minor Rb disorder components Rb (2) and Rb (3), which were refined isotropically. The largest residual electron density peak and hole in the final difference map are +2.77 and −0.96 $e^-/Å^3$, located 1.41 Å from Ga (3)/Ti (3) and 1.63 Å from O (1).

2.3. Energy dispersive spectroscopy (EDS)

EDS was performed on a colorless RGTO rod using a TESCAN Vega-3 SBU scanning electron microscope (SEM) with a Thermo EDS attachment operated in an ultralow vacuum mode. The crystal was mounted on a SEM stub with carbon tape and analyzed using the 20 kV accelerating voltage and an accumulation time of 20 s. EDS corroborated the presence of the elements in the composition obtained from the single crystal X-ray diffraction data and the absence of undesired extraneous elements such as silver from the reaction vessel.

2.4. First principles calculations

The DFT calculations were performed using the Vienna Ab-initio Package (VASP) code [22,23], with the generalized gradient approximation of Perdew, Burke and Ernzerhof (PBE) [24] and projector augmented wave (PAW) method [25,26]. To model the Ti/Ga mixing and partial occupies of the Rb atom, super quasi-random structure (SQS) was made with composition $Rb_{0.7}Ga_{6.6}Ti_{0.4}O_{11}$, with 5 unit cells in c-direction, ensuring widest distribution of Rb and Ti atoms (relaxed SQS are provided in the Supporting Information). To see if the SQS is thermodynamically stable, i.e., if it breaks the Rb–Ti-Ga-O convex hull, its formation energy was compared with respect to the Open Quantum Materials Database (OQMD) [27] convex hull. We used the OQMD calculations set-up: 520 eV cut-off energy for the plane wave basis set, 10^{-4} eV energy convergence criterion, 5 × 8 × 1 **k**-point mesh. For calculating the electronic and optical properties, more rigorous calculations were performed, using 520 eV cut-off energy for the plane wave basis set, 10^{-6} eV and 10^{-3} eV/Å energy and forces convergence criteria, respectively, and the same **k**-point mesh as the OQMD calculations. We also made two SQSs where Rb was replaced by K and Cs, to study the Rb ion exchange in the RGTO compound. For studying the influence of defects, we also made two structures where Ga was replaced by Fe and Co, to study the influence of magnetic elements on the properties of RGTO. The ground state geometries were obtained by relaxing the cell volume, cell shape and atomic positions. The adsorption index was obtained from the calculated frequency dependent dielectric function in the independent-particle picture.

3. Results and discussion

3.1. Synthesis and crystal structure

Mixed alkali halides are excellent fluxes that can dissolve a large number of oxide and fluoride reagents, and from which a wide variety of complex oxides can be grown as X-ray diffraction quality single crystals [28–30]. In these mixed halide solvent systems, a fluoride component is often employed to enhance the dissolution of oxide reagents by functioning as a mineralizer. This is especially true in the case of RGTO, where neither Ga_2O_3 nor TiO_2 can be readily dissolved by a pure alkali chloride melt; however, both dissolve well in a mixed chloride-fluoride melt. GaF_3 was chosen as the Ga source primarily due to its enhanced dissolution in a chloride-fluoride flux. This reaction, which targeted a Ga-based rubidium titanium hollandite [8], resulted in the crystallization of RGTO.

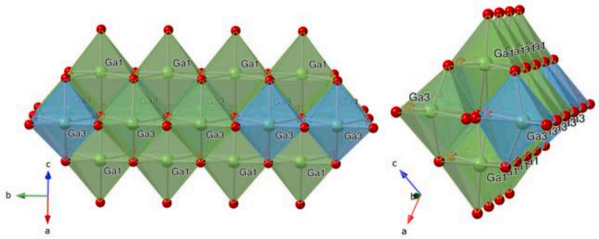

Fig. 1. A polyhedral representation of a column formed from Ga (1)O_6 and Ga/Ti (3)O_6 octahedra. Pure Ga and mixed Ga/Ti sites are shown in green and blue, respectively. Oxygen is shown in red. (For interpretation of the references to color in this figure legend, the reader is referred to the Web version of this article.)

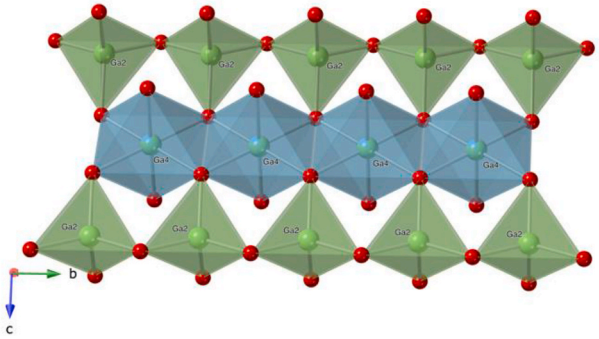

Fig. 2. An illustration of Ga (2)O_4 and Ga/Ti (4)O_6 sheet down the *a*-axis. Pure Ga and mixed Ga/Ti sites are shown in green and blue, respectively. Oxygen is shown in red. (For interpretation of the references to color in this figure legend, the reader is referred to the Web version of this article.)

A wide variety of oxides crystallize in the rutile structure type (space group $P4_2/mnm$) as well as in other closely related structure types [31]. A less common parent framework is that of β-Ga_2O_3. β-Ga_2O_3 crystallizes in the monoclinic space group $C2/m$ and features two gallium sites, octahedral and tetrahedral. The crystal structure of RGTO contains structural elements of the rutile, hollandite and β-Ga_2O_3 configurations, contained as columns that run along the crystallographic *c*-axis. It is interesting to note that similar structural aspects were observed in other closely related tunnel structures, $A_xGa_8Ga_{8+x}Ti_{16-x}O_{56}$ (A = K, Rb and Cs; x less than or equal to 2) [32]. Compared to the rutile or hollandite structure types that feature one unique mixed metal site, however, RGTO features four unique metal sites of which two are mixed (Ga/Ti) and two are pure gallium sites.

RGTO crystallizes in the monoclinic space group $P2/m$ with lattice parameters $a = 8.3355$ (8) (Å), $b = 3.0286$ (3) (Å), $c = 9.5028$ (9) (Å), and $\beta = 114.620$ (3)°. The structure of RGTO consists of Ga (1)O_6 and Ga/Ti (3)O_6 octahedra that form columns (Fig. 1) running down the *b*-axis. These columns are connected to sheets (Fig. 2) consisting of edge-sharing Ga/Ti (4)O_6 octahedra connected to Ga (2)O_4 tetrahedra via corner-sharing. This assembly of columns and sheets produces a complex three-dimensional structure containing tunnels running down the *b*-axis that are occupied by Rb cations that provide charge balance to the anionic framework, as shown in Fig. 3. The difference between the hollandite and the RGTO structure is manifested in the different channel sizes. Shown in Fig. 4 are cross sections of the channels and interatomic distances. The channels in the RGTO structure are roughly 1.5 Å larger than those in the hollandite structure, suggesting that the RGTO structure type can accommodate, in general, larger cations in the channels. This is an area that we will explore in the future.

Overall, the crystal structure of RGTO contains structural components that are clearly reminiscent of the rutile, hollandite, and β-Ga_2O_3 structure types (Fig. 5). Given the close similarity between aforementioned structures, similar syntheses may lead to other complex tunnel structures. Crystallographic refinement data for RGTO are provided in Table 1. Table 2 lists select interatomic bond distances.

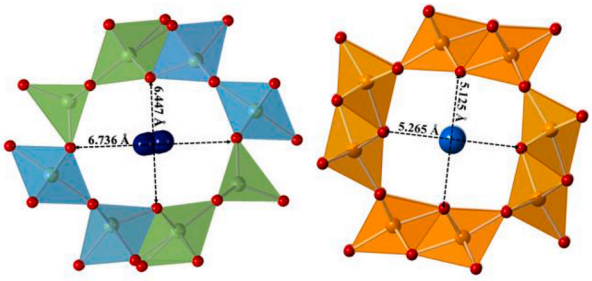

Fig. 4. Tunnel dimensions in Å of RGTO (left) and hollandite (right).

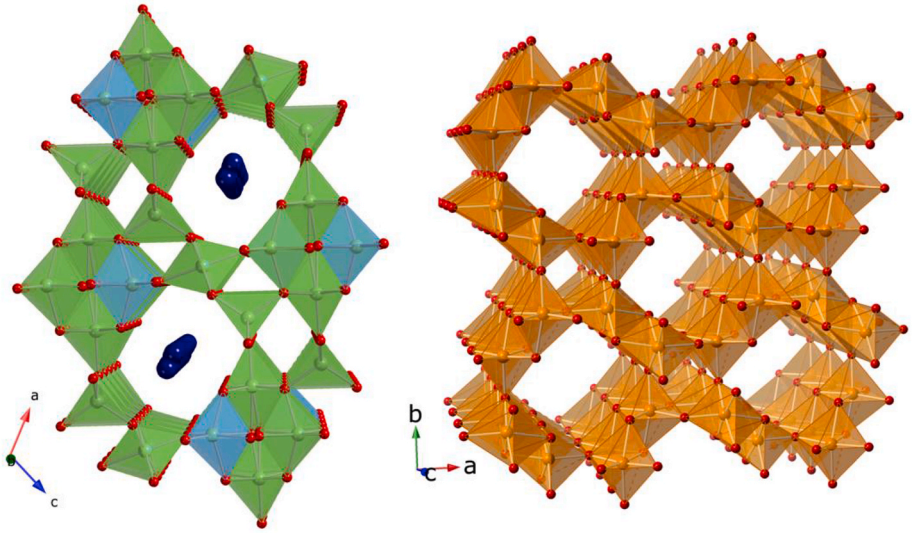

Fig. 3. Polyhedral representation of the crystal structure of RGTO (shown on the left) and its structural comparison to the hollandite ($A_xM_8O_{16}$) structure type (shown on the right). Rb, pure Ga and mixed Ga/Ti sites in RGTO are shown in deep blue, green and blue, respectively. Oxygen is shown in red. (For interpretation of the references to color in this figure legend, the reader is referred to the Web version of this article.)

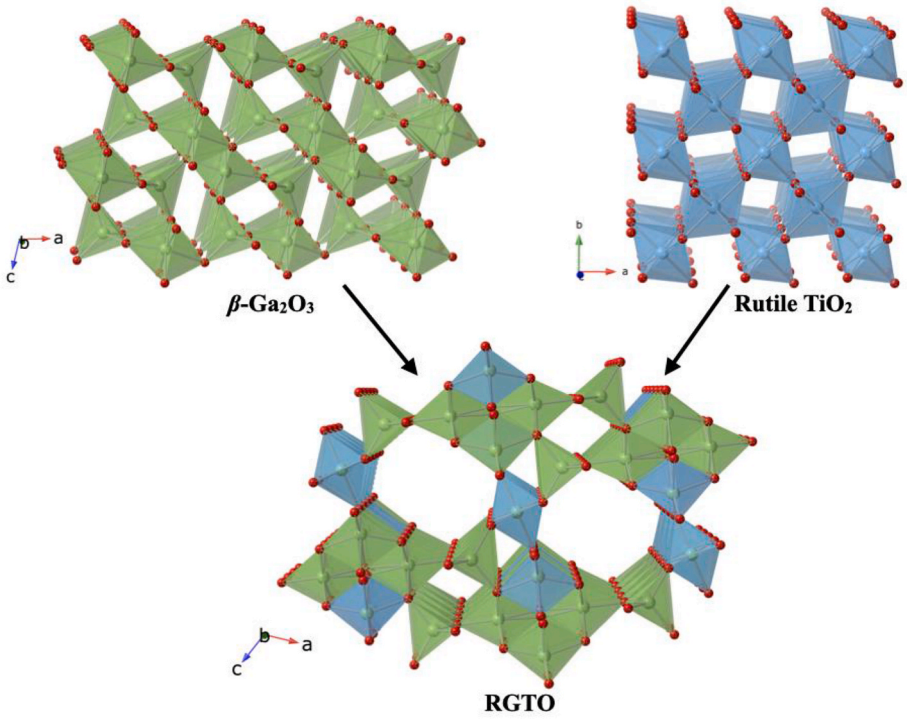

Fig. 5. Structural comparison of the β-Ga_2O_3 and rutile TiO_2 structure types to RGTO which contains structural elements of both: the corner sharing chains of edge sharing octahedra found in both Rutile and β-Ga_2O_3, the condensed chains of edge sharing octahedra found in β-Ga_2O_3, and the corner sharing chains of tetrahedra found in β-Ga_2O_3.

Table 1
Crystallographic and refinement data for $Rb_{0.74}Ga_{6.62}Ti_{0.38}O_{11}$.

Empirical formula	$Rb_{0.74}Ga_{6.62}Ti_{0.38}O_{11}$
Crystal color and habit	Colorless rod
Formula weight (g/mol)	718.55
Temperature (K)	301 (2)
Wavelength (Å)	0.71073
Crystal system	Monoclinic
Space group	*P2/m*
a (Å)	8.3355 (8)
b (Å)	3.0286 (3)
c (Å)	9.5028 (9)
β (deg.)	114.620 (3)
Volume (Å^3)	218.09 (4)
Z	1
Density (calculated) (Mg/m^3)	5.471
Absorption coefficient (mm^{-1})	24.598
Reflections collected	11,270
Independent reflections	1349 [R (int) = 0.0295]
Goodness-of-fit on F^2	1.129
R indices [I > 2σ(I)]	$R_1 = 0.0255$, w$R_2 = 0.0680$
R indices (all data)	$R_1 = 0.0273$, w$R_2 = 0.0690$
Largest diffraction peak and hole (e^-.A^{-3})	2.767 and −0.960

Table 2
Interatomic distances (Å) for $Rb_{0.74}Ga_{6.62}Ti_{0.38}O_{11}$. *M*(3) = Ga/Ti = 0.901/0.099; *M*(4) Ga/Ti = 0.817/0.183.

Ga (1)–O (1)	1.932 (2)
Ga (1)–O (2) x2	1.9433 (16)
Ga (1)–O (4) x2	2.0706 (17)
Ga (1)–O (6)	1.97 (2)
Ga (1)–O (6)	2.03 (2)
Ga (2)–O (1) x2	1.8327 (13)
Ga (2)–O (3)	1.814 (2)
Ga (2)–O (4)	1.880 (2)
M(3) – O (2)	1.887 (2)
M(3) – O (4)	1.998 (2)
M(3) – O (5) x2	1.8702 (15)
M(3) – O (6) x2	2.240 (9)
M(4) – O (3) x4	1.9939 (16)
M(4) – O (5) x2	1.975 (3)

The hollandite structure is well known for its ability to undergo ion exchange of the channel located cations. As RGTO is structurally related to the hollandite structure we attempted to exchange the rubidium cations in the RGTO tunnels with other alkali cations such as K and Cs. Single crystals of RGTO were soaked in molten ANO_3 (A = K and Cs) salt bath to determine if the Rb cations can be exchanged with other alkali cations; however, no ion exchange was observed. In our recent publication we reported on the successful ion exchange of Rb for Cs in $CsGa_7O_{11}$, as predicted by DFT calculations. To better understand why the ion exchange of K for Rb in $Rb_{0.74}Ga_{6.62}Ti_{0.38}O_{11}$ did not work, we again looked at the results from DFT calculations (vide infra). Finally, it is interesting to note that although the channel in RGTO is larger than the one found in the hollandite structure, it does not undergo ion exchange the way the hollandite structure does [33,34].

3.2. First principles calculations

To better understand why the ion exchange experiments failed, we used DFT calculations to determine the energetics of an alkali ion-exchange reaction, considering that the reaction is happening in an ANO_3 melt. The Rb/K ion-exchange energy is 0 meV, suggesting that there is some possibility for exchanging Rb with K, while the Rb/Cs ion-exchange energy is 61 meV, indicating that Rb should not exchange with Cs, where experimental results are consistent with these DFT results. Compared to the all gallium $CsGa_7O_{11}$ compound [9], the exchange of Rb with Cs is less favorable for the RGTO structure, coming from the more positive ion exchange energy for RGTO (61 meV) compared to $CsGa_7O_{11}$ (13 meV). Furthermore, for RGTO we determined that while in principle the ion exchange of K for Rb is possible coming from the ~0 eV ion exchange energy, still we should not be surprised that this ion

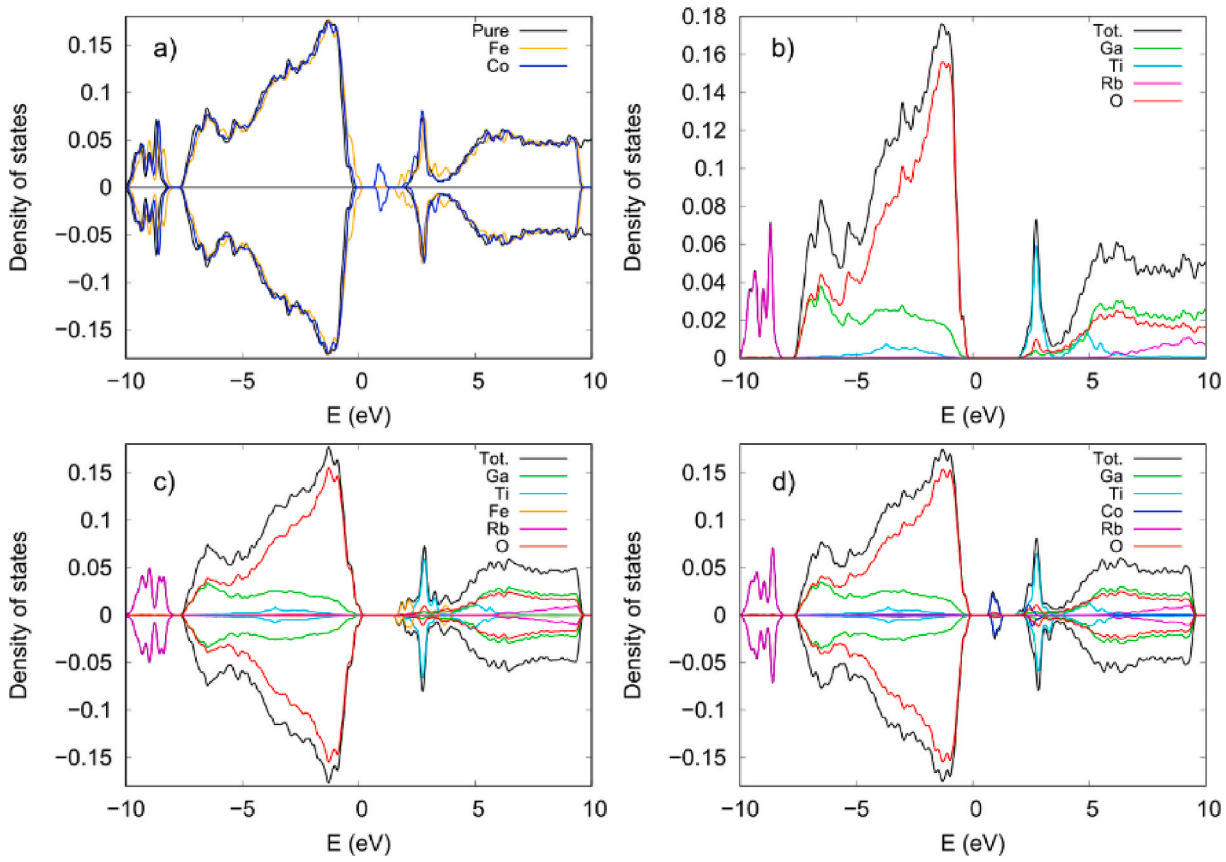

Fig. 6. a) total density of states (DOS) of pure RGTO (black), and RGTO with Fe (orange) and Co (blue) defects. Projected DOS (PDOS) of: b) pure RGTO, c) RGTO with Fe defect, and d) RGTO with Co defect. The PDOS coming from Ga, Ti, Fe, Co, Rb and O states are shown in green, cyan, orange, blue, magenta, and red, respectively. (For interpretation of the references to color in this figure legend, the reader is referred to the Web version of this article.)

exchange did not proceed experimentally.

Furthermore, DFT calculations show that the RGTO exists in a metastable state as its formation enthalpy is 8 meV above the Rb-Ga-Ti-O convex hull; however, this energy is small enough that a slight increase in temperature (~93 K) can stabilize the RGTO phase. To explore the potential of achieving additional elemental substitution in the RGTO framework, DFT calculations were carried out to assess this feasibility. For example, the process of exchanging Ga with Fe or Co in the RGTO structure was found to be energetically unfavorable, the formation energy for forming such substitutions are 2.306 and 2.544 eV/point defect for Fe and Co, respectively.

DFT clearly shows that RGTO is a charge transfer semiconductor, Fig. 6, indicated by the dominant O states at the top of the valence band and Ti states at the bottom of the conduction band, see Fig. 6b.

Overall, while RGTO is shown to be at least metastable by virtue of its synthesis, DFT calculations indicate that further modifications, such as exchanging the rubidium cations in the channels or the gallium with iron or cobalt in the framework, are energetically unfavorable.

4. Conclusion

Single crystals of the new pseudo-quaternary, $Rb_{0.74}Ga_{6.62}Ti_{0.38}O_{11}$, were obtained by molten RbCl–RbF eutectic flux synthesis at 850 °C. Single crystal X-ray diffraction determined that RGTO crystallizes in the monoclinic space group *P2/m*. The crystal structure of RGTO is a complex three-dimensional framework containing Rb cations in the tunnels for charge balance. RGTO forms in the $RbGa_7O_{11}$ structure type, which is reminiscent of the hollandite structure type. RGTO is predicted to be a charge transfer semiconductor based on the electronic structure calculations with O- and Ti-derived states contributing the most around the Fermi level. Ion exchange reactions were unsuccessful, most likely due to loss of thermodynamic stability as indicated by the DFT calculations.

Declaration of competing interest

The authors declare that they have no known competing financial interests or personal relationships that could have appeared to influence the work reported in this paper.

Acknowledgements

M.U., M.D.S., and H.Z.L. gratefully acknowledge the U.S. National Science Foundation, award OIA-1655740, for supporting the crystal growth, synthesis, and structure determination efforts. V.K. and T.M.B. acknowledge the support by the U.S. Department of Energy, Office of Science, Basic Energy Sciences, under Award No. DE-SC0016574 (Center for Hierarchical Waste Form Materials) for supporting the computational efforts. This research used computational resources provided by the National Energy Research Scientific Computing Center (NERSC) and the HPC cluster Hyperion, supported by The Division of Information Technology at the University of South Carolina.

Appendix A. Supplementary data

Supplementary data to this article can be found online at https://doi.org/10.1016/j.solidstatesciences.2020.106394.

References

[1] K. Hashimoto, H. Irie, A. Fujishima, Jpn. J. Appl. Phys. 44 (2005) 8269–8285.
[2] S.A. Campbell, D.C. Gilmer, X.C. Wang, M.T. Hsieh, H.S. Kim, W.L. Gladfelter, J. H. Yan, IEEE Trans. Electron. Dev. 44 (1997) 104–109.
[3] B. Oregan, M. Gratzel, Nature 353 (1991) 737–740.
[4] K. Maeda, ACS Appl. Mater. Interfaces 6 (2014) 2167–2173.
[5] K. Bange, C.R. Ottermann, O. Anderson, U. Jeschkowski, M. Laube, R. Feile, Thin Solid Films 197 (1991) 279–285.
[6] H.-C. zur Loye, T. Besmann, J. Amoroso, K. Brinkman, A. Grandjean, C.H. Henager, S. Hu, S.T. Misture, S.R. Phillpot, N.B. Shustova, H. Wang, R.J. Koch, G. Morrison, E. Dolgopolova, Chem. Mater. 30 (2018) 4475–4488.
[7] National Research Council, Waste Forms Technology and Performance: Final Report, The National Academies Press, Washington, DC, 2011, https://doi.org/10.17226/13100.
[8] J.V. Crum, L. Turo, B. Riley, M. Tang, A. Kossoy, J. Am. Ceram. Soc. 95 (4) (2012) 1297–1303.
[9] E.R. Vance, D.T. Chavara, D.J. Gregg, MRS Energy & Sustain. 4 (2017) 48.
[10] A.E. Ringwood, S.E. Kesson, N.G. Ware, W.O. Hibberson, A. Major, Geochem. J. 13 (4) (1979) 141–165.
[11] A.E. Ringwood, S.E. Kesson, N.G. Ware, W.O. Hibberson, A. Major, Nature 278 (1979) 219–223.
[12] J. Amoroso, J.C. Marra, M. Tang, Y. Lin, F. Chen, D. Su, K.S. Brinkman, J. Nucl. Mater. 454 (1–3) (2014) 12–21.
[13] S.A. Utlak, T.M. Besmann, K.S. Brinkman, J.W. Amoroso, J. Am. Ceram. Soc. 102 (10) (2019) 6284–6297.
[14] A.V. Knyazev, D.N. Demidov, A.A. Zhakupova, J. Solid State Chem. 286 (2020) 121295.
[15] C. Cao, K. Singh, W.H. Kan, M. Avdeev, V. Thangadurai, Inorg. Chem. 58 (8) (2019) 4782–4791.
[16] M. Usman, V. Kocevski, M.D. Smith, G. Morrison, T. Besmann, H.-C. zur Loye, Cryst. Growth Des. 20 (4) (2020) 2398–2405.
[17] C.A. Juillerat, V. Kocevski, V.V. Klepov, J.W. Amoroso, T. Besmann, H.-C. zur Loye, J. Am. Ceram. Soc. (2020), https://doi.org/10.1111/jace.17327 accepted.
[18] APEX3 Version 2016.5-0 and **SAINT**+ Version 8.37A, Bruker AXS, Inc., Madison, Wisconsin, USA, 2016.
[19] SADABS-2016/2, L. Krause, R. Herbst-Irmer, G.M. Sheldrick, D. Stalke, J. Appl. Crystallogr. 48 (2015) 3–10.
[20] (a) SHELXT, G.M. Sheldrick, Acta Crystallogr. A71 (2015) 3–8;
(b) SHELXL, G.M. Sheldrick, Acta Crystallogr. C71 (2015) 3–8.
[21] ShelXle: A Qt graphical user interface for SHELXL, C.B. Hübschle, G.M. Sheldrick, B. Bittrich, J. Appl. Crystallogr. 44 (2011) 1281–1284.
[22] G. Kress, J. Furthmüller, Phys. Rev. B 54 (1996) 11169–11186.
[23] G. Kress, J. Furthmüller, Comput. Mater. Sci. 6 (1996) 15–50.
[24] J.P. Perdew, K. Burke, M. Erzenhorf, Phys. Rev. Lett. 77 (1996) 3865–3868.
[25] P.E. Blöchl, Phys. Rev. B 50 (1994) 17953–17979.
[26] G. Kresse, D. Joubert, Phys. Rev. B 59 (1999) 1758–1775.
[27] J.E. Saal, S. Kirklin, M. Aykol, B. Meredig, C. Wolverton, JOM 65 (2013) 1501–1509.
[28] D.E. Bugaris, H.-C. zur Loye, Angew. Chem., Int. Ed. Engl. 51 (2012) 3780–3811.
[29] M. Usman, M.D. Smith, V. Kocevski, T. Besmann, H.-C. zur Loye, CrystEngComm 22 (2020) 1112–1119.
[30] M. Usman, G.B. Ayer, M.D. Smith, H.-C. zur Loye, J. Chem. Crystallogr. (2020), https://doi.org/10.1007/s10870-020-00834-5.
[31] W.H. Baur, Acta Crystallogr. 9 (1956) 515–520.
[32] Y. Fujuki, M. Watanabe, T. Sasaki, S. Takenouchi, J. Ceram. Soc. Jpn. 98 (1143) (1990) 1245–1249.
[33] Y. Kadoma, S. Oshitari, K. Ui, N. Kumagai, Electrochim. Acta 53 (4) (2004) 1697–1702.
[34] N. Kumagai, S. Oshitari, S. Komaba, Y. Kadoma, J. Power Sources 174 (2) (2007) 932–937.